PROCEEDINGS OF SPIE

SPIEDigitalLibrary.org/conference-proceedings-of-spie

Phantom and methodology for fluorescence molecular imaging systems benchmarking

D. Gorpas, M. Koch, M. Anastasopoulou, U. Klemm, V. Ntziachristos

D. Gorpas, M. Koch, M. Anastasopoulou, U. Klemm, V. Ntziachristos, "Phantom and methodology for fluorescence molecular imaging systems benchmarking," Proc. SPIE 10677, Unconventional Optical Imaging, 106771G (24 May 2018); doi: 10.1117/12.2309766



Event: SPIE Photonics Europe, 2018, Strasbourg, France

Phantom and methodology for fluorescence molecular imaging systems benchmarking

D. Gorpas*a,b, M. Kocha,b, M. Anastasopouloua,b, U. Klemmb, V, Ntziachristos*a,b

a Technical University Munich, Chair for Biological Imaging, Arcisstrasse 21, Munich D-80333,

Germany

^b Helmholtz Zentrum München, Institute for Biological and Medical Imaging, Ingolstädter Landstrasse 1, Neuherberg D-85764, Germany

dimitrios.gkorpas@tum.de and v.ntziachristos@tum.de

Abstract

A critical issue associated with the clinical translation of fluorescence molecular imaging relates to the reproducibility of the collected measurements. In particular, images acquired from the same target using different fluorescence cameras may vary considerably when the employed systems have markedly different specifications. Methods that standardize fluorescence imaging are therefore becoming necessary for assessing the performance of fluorescence systems and agents and for providing a reference to the data collected. In the work presented herein we propose a composite phantom for integrating multiple targets within the field of view of a fluorescence camera. Each quadrant of this phantom resolves different fluorescence features: (1) sensitivity as a function of the optical properties; (2) sensitivity as a function of the depth from the top surface; (3) resolution of the fluorescence and optical imaging; and (4) cross-talk from the excitation light. In addition, there exist structures in the phantom for assessing homogeneity of the incident illumination. In order to validate our main hypothesis that standardization of fluorescence imaging systems is feasible through imaging such a phantom, we employed two systems of different specifications and quantified all relevant performance metrics. The derived results showcase the feasibility of fluorescence cameras calibration. Additionally, we demonstrate a methodology of comparing fluorescence cameras by means of benchmarking scoring. We expect that such approaches will boost the clinical translation of fluorescence molecular imaging and will allow for the investigation of novel fluorescence agents.

Keywords: Fluorescence imaging, standardization, camera calibration

1. INTRODUCTION

Fluorescence imaging has shown evidence for positively impacting the clinical management and prognosis of numerous diseases. Nevertheless, images acquired from the same fluorescent target using different cameras may vary considerably when the employed systems present markedly different specifications. This is one of the limiting factors that delay the clinical translation of this technology.

Therefore, methods that standardize fluorescence imaging are becoming necessary for assessing the performance of fluorescence systems and agents and for providing a reference to the recorded data. Up to date, comparison of imaging systems has been achieved by numerous phantoms proposed ¹⁻⁴. The sensitivity of fluorescence cameras and the excitation light leakage into the acquired fluorescence images were recently assessed through polyurethane-based phantoms ^{1, 2}. Other proposed phantoms include tissue-mimicking phantoms that simulate optical properties and/or geometry of sample tissues and have been applied mostly for training surgeons or as hardware and/or software validation targets ^{3, 5, 6}. Nevertheless, the number of the resolved performance parameters derived from these phantoms do not allow for comprehensive characterization of all variables associated with fluorescence imaging performance.

Recently we proposed a composite phantom that integrates multiple targets within the field of view of a fluorescence camera ⁷. In the work presented herein we sought to introduce a methodology that has the potential to standardize fluorescence cameras through a single or a few image acquisitions of the phantom. We show, for the first time, how composite phantoms can be employed for comparing systems of different specifications. The described benchmarking method may become critical for standardization of imaging systems with broader applications for clinical translation of fluorescence molecular imaging.

2. METHODS

2.1 Phantom

We have previously proposed a composite phantom for interrogating different aspects of fluorescence and optical imaging performance ⁷. The phantom consists of a number of imaging targets and resolves different fluorescence features (Fig. 1). In particular, as shown in Fig. 1, each quadrant of the phantom tests different performance parameters, i.e., (1) sensitivity as a function of the optical properties (red color); (2) sensitivity as a function of the depth from the top surface (blue color); (3) resolution of the fluorescence and optical imaging (purple color); and (4) cross-talk from the excitation light (pink color). The five wells at the corners and center of the phantom (green color) have been added to assess the field illumination (i.e., illumination for enabling reflectance color imaging) homogeneity when optical measurements are performed through a color camera.

The main materials used for the development of the phantom are transparent polyurethane (WC-783 A/B, BJB Enterprises, Tustin, United States) for the phantom matrix, organic quantum dots (Qdot® 800 ITKTM, Q21771MP, Thermofisher Scientific Waltham, United States) for fluorescence targets, anatase TiO2 nanoparticles (Titanium IV Oxide, Sigma Aldrich, St. Louis, United States) for scattering, and alcohol soluble nigrosin (Sigma Aldrich) in the phantom main body and Hemin (Sigma Aldrich, from bovine ≥90%) in the different wells for absorption. The stability of their optical properties over time and their ability to create homogeneous mixtures were the main factors for choosing these materials ^{2,7}. The procedure of the phantom's preparation has been explicitly described elsewhere ⁷.

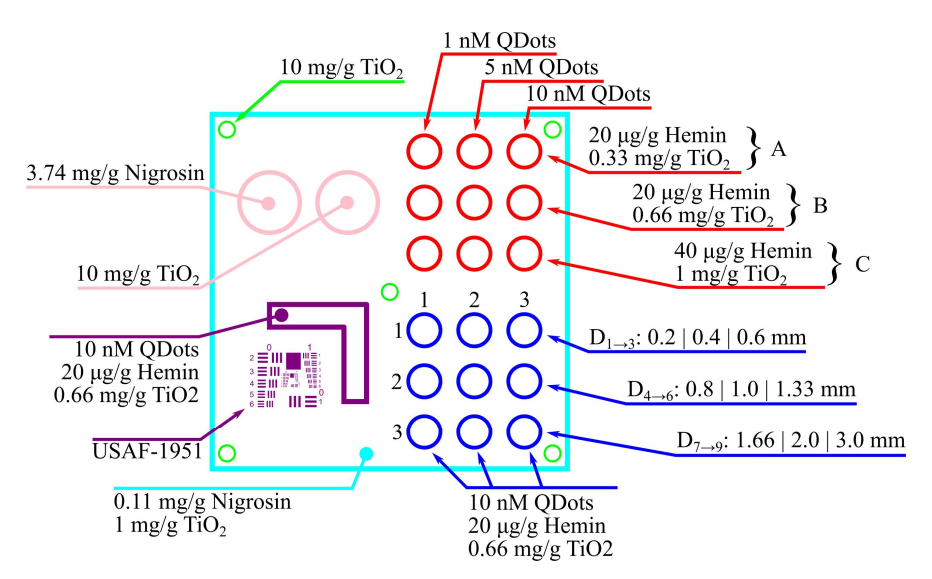


Fig. 1 The standardization phantom employed in this study. The different compartments per element and/or group of elements of the phantom. The base material is transparent rigid polyurethane. Arrowheads indicate that a group of elements (per row, column, or color code) have the same constituents, while the dotheads indicate the composition of a single element of the phantom. Color codes: red—sensitivity versus optical properties (three sets of optical properties, A, B, and C); blue—sensitivity versus depth (index in the 3 × 3 matrix defines the depth); purple—resolution; pink—cross-talk; green—field illumination homogeneity; cyan—phantom body; Di—depth from the phantom's top surface.

2.2 Phantom imaging

To test the composite phantom for comparing fluorescence cameras with markedly different specifications two acquisition parameters were investigated: (1) pixel-binning of the camera sensor and (2) working distance. For all experiments performed, fluorescence was enabled by the same excitation source, that is, the 750-nm laser diode (BWF2-750-0, B&W Tek, Newark, Delaware, United States), and images were acquired with room lights turned off. The integration time was set at 0.1 s, to resemble realtime measurements as they are performed in vivo. To ensure minimization of boundary effects, the phantom was placed on top of a highly absorbing material.

To examine the effects of pixel-binning, the two cameras used were positioned at the same 320-mm working distance from the phantom surface. This distance is a representative working distance for a wide range of intraoperative

applications. Fluorescence images were then acquired at various gains, cooling temperatures, and pixel binning settings

The system in Fig. 2 (camera I) is a modified version of the one that has been developed, characterized, and reported by our group elsewhere ⁹. Briefly, the 750-nm CW laser is used to excite the fluorescence compounds of the phantom, while white-light illumination is enabled by a 250-W halogen lamp (KL-2500 LCD, Schott AG, Mainz, Germany). Ground glass diffusers (DG10-220, Thorlabs, Newton, New Jersey, United States) are used to achieve uniform illumination of the field of view from both light sources. The optical signal is collected by a motorized zoom/focus lens (CVO GAZ11569M, Goyo Optical Inc., Asaka, Saitma, Japan) and spectrally resolved in two channels by a dichroic mirror (700DCXXR, AHF analysentechnik AG, Tubingen, Germany). The first channel is within the spectral range from 720 to 850 nm, filtered by a NIR emission filter (ET810/90, Chroma Technology), and recorded by an iXon electron multiplying charge-coupled device (EMCCD, DV897DCS-BV, Andor Technology, Belfast, Northern Ireland). The second channel is within the spectral range 450 to 700 nm, relayed through a visible achromatic doublet pair (MAP10100100-A, Thorlabs), and recorded by a 12-bit color charge-coupled device (CCD) camera (pixelfly qe, PCO AG, Kelheim, Germany).

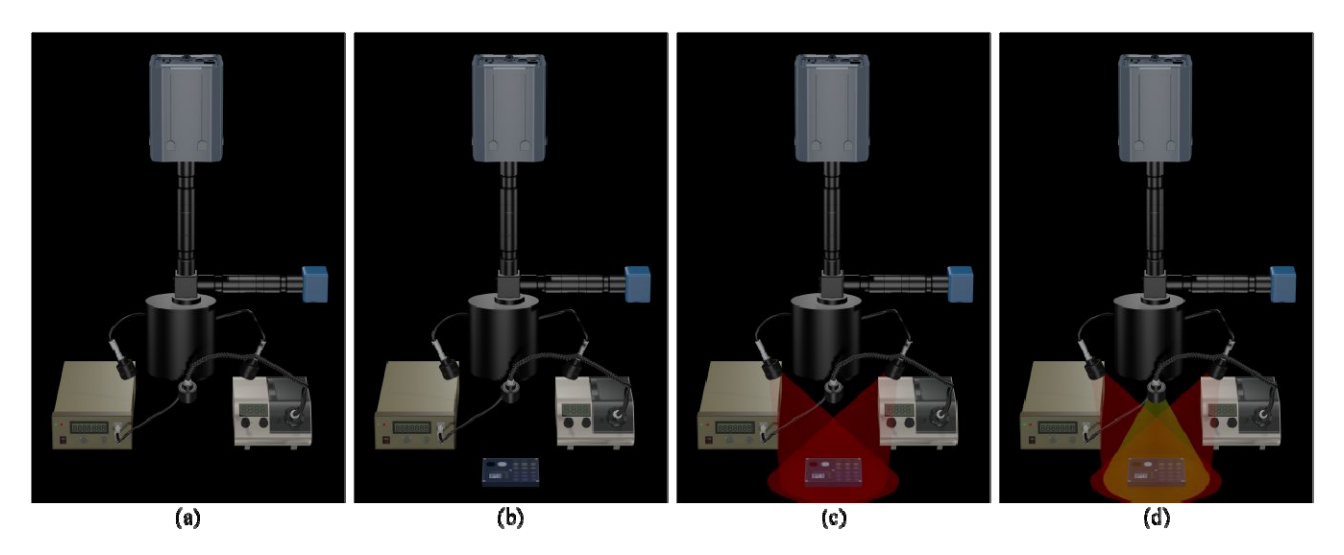


Fig. 2 Camera I acquisition protocol. (a) Camera I is prepared for imaging at desired working distance. (b) Phantom is placed within the field of view. (c) Fluorescence acquisition is enabled by a 750 nm CW laser diode. (d) Field illumination enables acquisition of concurrent to fluorescence color images.

The second system (camera II) is also based on EMCCD detection (Luca R, Andor Technology). Camera II has four major differences compared to camera I: (1) it lacks the color imaging channel (450- to 700-nm spectral band), (2) it has different operational characteristics (16×16 µm pixel size of camera I vs 8×8 µm of camera II, ~70% QE of camera I vs ~40% QE of camera II at 800 nm), (3) it uses a different fluorescence filter (D850/40 m, Chroma Technology), and (4) it employs a different lens (Zoom 7000 Macro Lens, Navitar, New York, United States). Acquisition of phantom images with camera II is equivalent to the protocol adopted for camera I and shown in Fig. 2.

2.3 Image processing

We developed an automated method for the detection of all the composite phantom elements. This method employed the speeded-up robust features (SURF) algorithm ¹⁰ for both the acquired images and specially designed templates. The distance between the two sets of features was then computed and thresholded based on an efficient approximate nearest neighbor search ¹¹. The geometric transformation between the acquired images and the templates was then exported by the conjugate points resulting from the afore mentioned distance estimation ⁸.

Following the estimation of the geometric transformation, predefined points of interest were projected from the templates onto the acquired images. These points include (1) the four corners of the phantom, (2) the center and one perimeter point of all the circular phantom elements, (3) the six corners of the L-shaped phantom element, and (4) the

four corners of the USAF-1951 target, as well as the four corners of all the target's line elements. With this points complete and comprehensive analysis of the acquired phantom images is feasible by means of magnification, optical resolution, diffused fluorescence resolution, excitation light leakage and parasitic illumination, sensitivity and field illumination homogeneity as described in ⁸.

Data acquisition and control of cameras were enabled via the Solis software (Solis I, Andor Technology) and a GPU-based C++ software developed by our group ⁹. All data processing was implemented in MATLAB (Mathworks Inc., Massachusetts, United States).

3. RESULTS

Some representative results of the comparison procedure are shown in Fig. 3. The phantom elements as automatically extracted from a fluorescence image acquired by camera I are shown in Fig. 3a. The adopted color-code for depicting the elements boundaries corresponds to the color-code of Fig. 1. Having all elements of the phantom available quantification of the various performance metrics is straightforward. The photon counts from the wells assessing sensitivity as a function of optical properties and depth are shown in Fig. 3a (left). Equivalent results from camera II are shown in Fig. 3b.

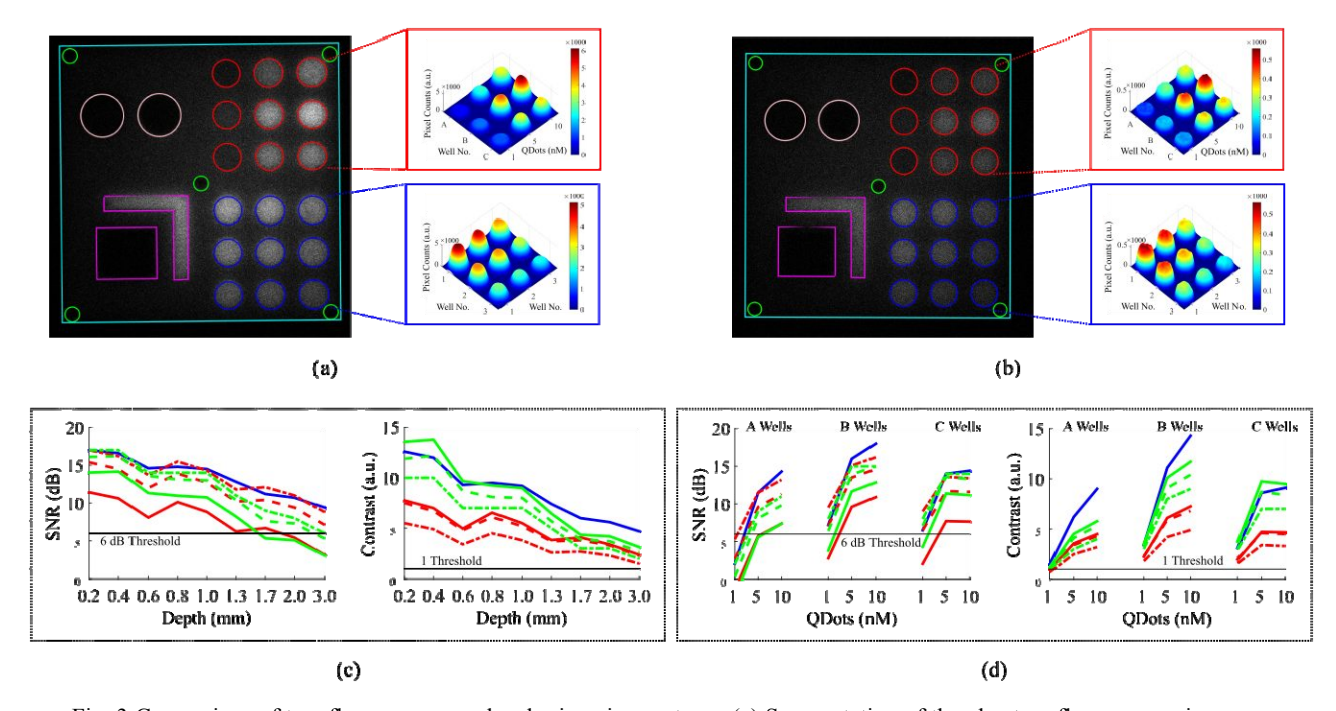


Fig. 3 Comparison of two fluorescence molecular imaging systems. (a) Segmentation of the phantom fluorescence image as acquired by camera I and photon counts from the wells that assess sensitivity as function of optical properties (top) and depth (bottom). (b) Segmentation of the phantom fluorescence image as acquired by camera II and photon counts from the wells that assess sensitivity as function of optical properties (top) and depth (bottom). (c) Assessment of sensitivity as a function of depth by means of signal to noise ratio (left) and contrast (right) for camera I and camera II under various acquisition settings. (d) Assessment of sensitivity as a function of optical properties by means of signal to noise ratio (left) and contrast (right) for camera I and camera II under various acquisition settings. In (c) and (d): - camera I; - camera II, - camera II with 2× binning; -- camera II with 4× binning; - camera II at 200 mm working distance; -- camera II at 200 mm working distance and 2× binning.

The signal to noise ratio and contrast can further be quantified and employed to compare two systems of markedly different specifications, like camera I and camera II. Figs. 3(c) and 3(d) depict those metrics for the wells assessing sensitivity as a function of depth and optical properties, correspondingly. Considering that camera I has been employed in the operating room for intraoperative fluorescence image guided surgery ¹²⁻¹⁴, we explored the performance of camera II as a function of pixel binning and working distance. Adopting a least squares method between all metrics quantified through the phantom we identified that camera II under 2× binning and with reduced working distance (200 mm *vs* 320

mm of camera I) is the one that approaches better the performance of camera I. Such benchmarking procedures can extend to multiple imaging systems and, based on the application, to weighted performance metrics contributions.

Besides comparing performance of different systems, the phantom described herein can also be employed to calibrate a fluorescence camera. Representative results are shown in Fig. 4, where correction for the field illumination inhomogeneity is shown in Fig. 4a and registration between the fluorescence and color channels of camera I is shown in Fig. 4b.

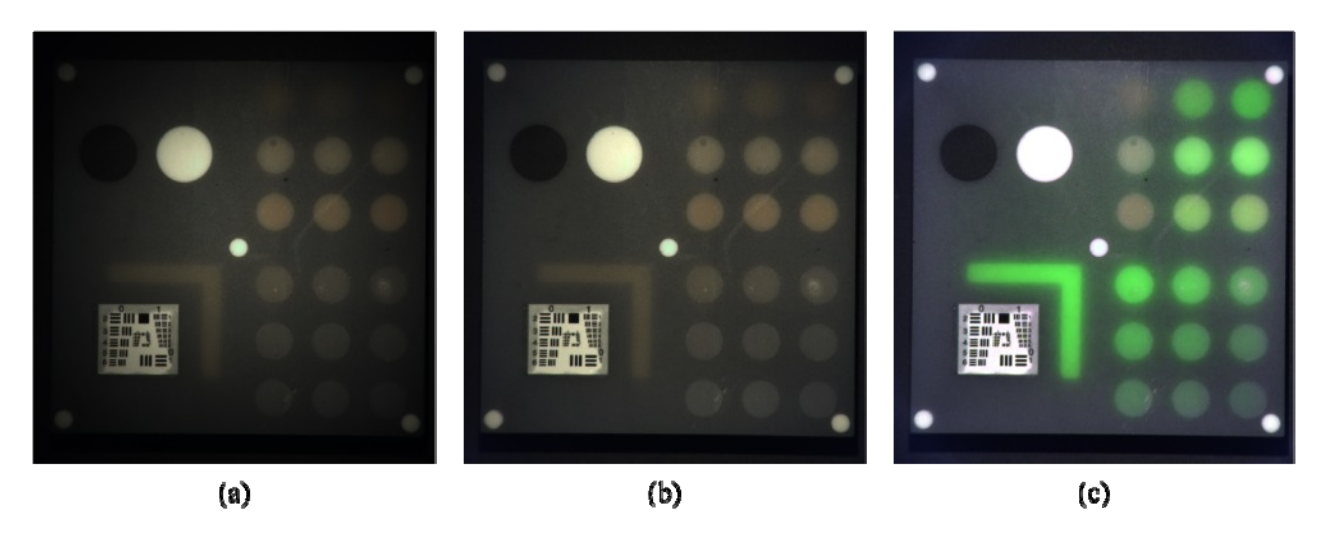


Fig. 4 Calibration of a hybrid fluorescence/color imaging system. (a) Acquired color phantom image. The field illumination inhomogeneity is appreciated by the strong presence of vignetting. (b) Corrected color image by performing flat-fielding

based on the scattering wells located at the corners and center of the phantom. Vignetting is removed without degrading the color information of the image. (c) Registered fluorescence and color channels of a hybrid system (camera I) expressed as composite image with fluorescence information overlaid onto the color image.

4. DISCUSSION

Lack of fluorescence imaging standardization is one of the major factors delaying clinical translation of this exciting technology ^{1, 15}. Most current approaches quantify one performance parameter ¹. The study herein introduced a multiparametric phantom for the characterization of fluorescence imaging systems based on the (a) automatic characterization of the performance of different imaging cameras and (b) calibration of two imaging platforms. The latter is essential for multicenter clinical trials. We envision that composite phantoms will become important assets for clinical translation of fluorescence molecular imaging.

The results presented in this study allowed the comparison of the two exemplary cameras employed herein for demonstration purposes and clearly indicated a superiority of camera I compared to camera II when operating at equivalent settings (i.e., working distance, pixel-binning, or gain, to name a few). However, modification of one or more of these acquisition parameters impacts imaging performance. Indeed, our results clearly demonstrate that appropriate adjustment of camera II acquisition parameters can modify the performance and optimize certain performance features to resemble camera I performance.

Future work includes the development of composite phantoms that can capture a larger number of camera parameters, such as characterizing the dynamic range and spectral response, and to offer a more accurate correction for inhomogeneous illumination. We plan to develop phantoms that will incorporate a number of wells within highly absorbing base material and thus, cross-talks between neighboring elements will be eliminated, whereas other wells will be within highly scattering base material, and thus allow for validation of the aforementioned systems. Functions for the automatic extraction of these additional features can then be developed to streamline the detection and analysis of a larger set of calibration parameters. Although there exists evidence in literature regarding the stability of the employed

materials ^{2, 7}, we further plan to perform systematic constancy and mechanical integrity tests to validate the stability of the optical properties of the various phantom elements at different environments.

Current study represents an early attempt of standardizing imaging measurements or systems for fluorescence molecular imaging. Overall, we expect that the field of standardization will play a major role in the growth of fluorescence molecular imaging and we foresee that composite phantoms will be a significant part of it.

ACKNOWLEDGEMENTS

The authors would like to thank Dr. Pilar Beatriz Garcia-Allende for her contribution during the preparation of the phantom. The research leading to these results has received funding by the Deutsche Forschungsgemeinschaft (DFG), Sonderforschungsbereich-824 (SFB-824), subproject A1 and from the European Union's Horizon 2020 research and innovation programme under the Marie Sklodowska-Curie grant agreement No. 644373 (PRISAR).

REFERENCES

- [1] Zhu B., Rasmussen J. C., and Sevick-Muraca E. M., "A matter of collection and detection for intraoperative and noninvasive near-infrared fluorescence molecular imaging: To see or not to see?," Med. Phys. **41**(2), 022105 (2014).
- [2] Zhu B., Tan I. C., Rasmussen J. C., and Sevick-Muraca E. M., "Validating the sensitivity and performance of near-infrared fluorescence imaging and tomography devices using a novel solid phantom and measurement approach," Technol. Cancer. Res. Treat. 11(1), 95-104 (2012).
- [3] Leh B., Siebert R., Hamzeh H., Menard L., Duval M.-A., Charon Y., and Abi Haidar D., "Optical phantoms with variable properties and geometries for diffuse and fluorescence optical spectroscopy," J. Biomed. Opt. 17(10), 108001 (2012).
- [4] Pogue B. W., and Patterson M. S., "Review of tissue simulating phantoms for optical spectroscopy, imaging and dosimetry," J. Biomed. Opt. 11(4), 041102 (2006).
- [5] Szyc Ł., Bonifer S., Walter A., Jagemann U., Grosenick D., and Macdonald R., "Development of a handheld fluorescence imaging camera for intraoperative sentinel lymph node mapping," J. Biomed. Opt. **20**(5), 051025 (2015)
- [6] Pleijhuis R. G., Langhout G. C., Helfrich W., Themelis G., Sarantopoulos A., Crane L. M. A., Harlaar N. J., de Jong J. S., Ntziachristos V., and van Dam G. M., "Near-infrared fluorescence (nirf) imaging in breast-conserving surgery: Assessing intraoperative techniques in tissue-simulating breast phantoms," Eur. J. Surg. Oncol. 37(1), 32-39 (2011).
- [7] Anastasopoulou M., Koch M., Gorpas D., Karlas A., Klemm U., Garcia-Allende P. B., and Ntziachristos V., "Comprehensive phantom for interventional fluorescence molecular imaging," J. Biomed. Opt. **21**(9), 091309 (2016)
- [8] Gorpas D., Koch M., Anastasopoulou M., Klemm U., and Ntziachristos V., "Benchmarking of fluorescence cameras through the use of a composite phantom," J Biomed Opt **22**(1), 016009 (2017).
- [9] Glatz J., Varga J., Garcia-Allende P. B., Koch M., Greten F. R., and Ntziachristos V., "Concurrent video-rate color and near-infrared fluorescence laparoscopy," J. Biomed. Opt. **18**(10), 101302 (2013).
- [10] Bay H., Ess A., Tuytelaars T., and Van Gool L., "Speeded-up robust features (surf)," Comput. Vis. Image Und. 110(3), 346-359 (2008).
- [11] Muja M., and Lowe D. G., Fast approximate nearest neighbors with automatic algorithm configuration. International Conference on Computer Vision Theory and Applications, 331-340 (2009).
- van Dam G. M., Themelis G., Crane L. M. A., Harlaar N. J., Pleijhuis R. G., Kelder W., Sarantopoulos A., de Jong J. S., Arts H. J. G., van der Zee A. G. J., Bart J., Low P. S., and Ntziachristos V., "Intraoperative tumor-specific fluorescence imaging in ovarian cancer by folate receptor-[alpha] targeting: First in-human results," Nat. Med. 17(10), 1315-1319 (2011).
- [13] Koch M., de Jong J. S., Glatz J., Symvoulidis P., Lamberts L. E., Adams A. L. L., Kranendonk M. E. G., Terwisscha van Scheltinga A. G. T., Aichler M., Jansen L., de Vries J., Lub-de Hooge M. N., Schröder C. P., Jorritsma-Smit A., Linssen M. D., de Boer E., van der Vegt B., Nagengast W. B., Elias S. G., Oliveira S.,

- Witkamp A. J., Mali W. P. T. M., Van der Wall E., Garcia-Allende P. B., van Diest P. J., de Vries E. G. E., Walch A., van Dam G. M., and Ntziachristos V., "Threshold analysis and biodistribution of fluorescently labeled bevacizumab in human breast cancer," Cancer Res 77(3), 623 (2017).
- [14] Lamberts L. E., Koch M., de Jong J. S., Adams A., Glatz J., Tranendonk M. E. G., Terwisscha van Scheltinga A. G. T., Jansen L., de Vries J., Lub-de Hooge M. N., Schroder C. P., Jorritsma-Smit A., Linssen M. D., de Boer E., van der Vegt B., Nagengast W. B., Elias S. G., Oliveira S., Witkamp A., Mali W. P. T. M., van der Wall E., Van Diest P. J., de Vries E. G., Ntziachristos V., and van Dam G. M., "Tumor-specific uptake of fluorescent bevacizumab-irdye800cw microdosing in patients with primary breast cancer: A phase i feasibility study," Clin Cancer Res 23(11), 2730-2741 (2017).
- [15] Koch M., and Ntziachristos V., "Advancing surgical vision with fluorescence imaging," Annu Rev Med 67(1), 153-164 (2016).